Atmos. Chem. Phys. Discuss., 9, 27611–27648, 2009
www.atmos-chem-phys-discuss.net/9/27611/2009/

Atmospheric Chemistry and Physics Discussions

This discussion paper is/has been under review for the journal Atmospheric Chemistry and Physics (ACP). Please refer to the corresponding final paper in ACP if available.

Can a global model chemical mechanism reproduce NO, NO_2, and O_3 measurements above a tropical rainforest?

R. C. Pike[1], J. D. Lee[2], P. J. Young[1,*], S. Moller[3], G. D. Carver[1,4], X. Yang[1], P. Misztal[5,6], B. Langford[7], D. Stewart[8,], C. E. Reeves[8], C. N. Hewitt[7], and J. A. Pyle[1,4]**

[1]Centre for Atmospheric Science, Department of Chemistry, University of Cambridge, Lensfield Road, Cambridge, CB2 1EW, UK
[2]National Centre for Atmospheric Science (NCAS), University of York, Heslington, York, YO10 5DD, UK
[3]Department of Chemistry, University of York, Heslington, York, YO10 5DD, UK
[4]National Centre for Atmospheric ScienceClimate, University of Cambridge, Lensfield Road, Cambridge, CB2 1EW, UK
[5]Centre for Ecology and Hydrology Edinburgh, Bush Estate, Penicuik, Midlothian, EH26 0QB, UK
[6]The University of Edinburgh, School of Chemistry, Joseph Black Building, West Mains Road, Edinburgh, EH9 3JJ, UK

[7] Lancaster Environment Centre, Lancaster University, Lancaster, LA1 4YQ, UK
[8] School of Environmental Sciences, University of East Anglia, Norwich, NR4 7TJ, UK
[*] now at: NOAA Earth System Research Laboratory, 325 Broadway, Boulder, CO, 80501, USA
[**] now at: Department of Chemistry, University of Reading, Whiteknights, Reading, RG6 6AH, UK

Received: 24 November 2009 – Accepted: 30 November 2009
– Published: 21 December 2009

Correspondence to: R. C. Pike (rachel.pike@atm.ch.cam.ac.uk)

Published by Copernicus Publications on behalf of the European Geosciences Union.

Abstract

A cross-platform field campaign, OP3, was conducted in the state of Sabah in Malaysian Borneo between April and July of 2008. Among the suite of observations recorded, the campaign included measurements of NO_x and O_3–crucial outputs of any model chemistry mechanism. We describe the measurements of these species made from both the ground site and aircraft. We examine the output from the global model p-TOMCAT at two resolutions for this location during the April campaign period. The models exhibit reasonable ability in capturing the NO_x diurnal cycle, but ozone is overestimated. We use a box model containing the same chemical mechanism to explore the weaknesses in the global model and the ability of the simplified global model chemical mechanism to capture the chemistry at the rainforest site. We achieve a good fit to the data for all three species (NO, NO_2, and O_3), though the model is much more sensitive to changes in the treatment of physical processes than to changes in the chemical mechanism. Indeed, without some parameterization of the nighttime boundary layer-free troposphere mixing, a time dependent box model will not reproduce the observations. The final simulation uses this mixing parameterization for NO and NO_2 but not O_3, as determined by the vertical structure of each species, and matches the measurements well.

1 Introduction

A four month field campaign, part of the NERC-funded "Oxidant and Particle Photochemical Processes" (OP3)[1], was conducted in the Malaysian state of Sabah, on the island of Borneo, between April and July of 2008 (for more information, see Hewitt et al., 2009b). There were two intensive periods of observation, the first between 8 April and 3 May, and the second between 25 June and 23 July. A key goal of the project is to assess our understanding of photochemical processes above a rainforest and their

[1]More information on OP3 can be found online at: http://www.es.lancs.ac.uk/op3/

impacts on various scales; to this end, the campaign utilized simultaneous ground, airborne, and satellite measurements (for a full list of instrumentation see Hewitt et al., 2009b). A further aim is to understand the scale relationships of these measurements as they are used by and contribute to mesoscale, regional, and global models.

Atmospheric oxidation above a tropical rainforest is complex (e.g. Kuhn et al., 2007; Lelieveld et al., 2008), and it is therefore beyond current computational resources to represent it explicitly in a global model. Furthermore, the horizontal resolution of the current generation of global models is 2–5° (approximately equivalent to 220 and 550 km at the equator, Stevenson et al., 2006), which limits their ability to model subgrid scale processes such as emission variability. At the same time, these models attempt to simulate the production and destruction of ozone, which is dependent on local chemical conditions (Crutzen, 1973; Sillman et al., 1990; Jenkin and Clemitshaw, 2000). Ozone is important for radiation (Gauss et al., 2006), and at high concentrations is detrimental to both human (Wilkins et al., 2001; Jerrett et al., 2009) and crop health (van Dingenen et al., 2009). Our understanding of the future impacts of ozone very often relies on the output of global models (Forster et al., 1996; Fuglestvedt et al., 1999; Stevenson et al., 2006) and it is therefore essential to understand how global chemical mechanisms perform in relation to the local measurements which help to constrain them.

Production of tropospheric ozone is non-linear (Liu et al., 1987; Jenkin and Clemitshaw, 2000), and depends largely on local concentrations of volatile organic compounds (VOC), the hydroxyl radical (OH), and the oxides of nitrogen (NO + NO_2 = NO_x) (e.g. Sillman, 1995). NO and NO_2 act as catalysts in many oxidation cycles in the atmosphere due to their rapid interconversion; the availability of NO_x largely determines whether ozone production or destruction dominates in a specific region of the tropical boundary layer (Liu et al., 1987), and the impact of NO_x on ozone production in the observation region has been previously described (Hewitt et al., 2009a). Photolysis of NO_2 is the only known production mechanism for ozone, while loss occurs through photochemical reaction with other trace gases and deposition to surfaces such

as the ocean or vegetation. Ozone can also be entrained into the troposphere from the ozone-rich stratosphere (Holton et al., 1995). The lifetime of tropospheric ozone is a few weeks to a month, depending on location in the atmosphere (e.g. Stevenson et al., 2006; Wild, 2007), and as such transport from the free troposphere may influence local boundary layer measurements of ozone.

Nitrogen oxides are emitted both by natural processes and human activities. Of the natural sources, emission from soils (Yienger and Levy II, 1995; Delon et al., 2008) and formation during lightning storms (Franzblau and Popp, 1989; Schumann and Huntrieser, 2007) are the major contributors. Fossil fuel combustion, biomass burning and aircraft emissions are the major anthropogenic sources (Kasibhatla, 1993; Levy II et al., 1999; Toenges-Schuller et al., 2006). Though fluxes from tropical areas are not yet well constrained, the work of Bakwin et al. (1990) suggested significant emissions from tropical forested areas. Jaeglé et al. (2004) reported that soil emissions could be as large as biomass burning emissions in Africa. In these remote tropical areas the potential for NO_x species to influence local chemistry is significant due to low background NO_x and high concentrations of both the hydroxyl radical and biogenic VOC (Steinkamp et al., 2009). An increase in the frequency and spatial distribution of tropical NO_x measurements will help quantify local tropical fluxes and sources. But global models will largely play the role of quantifying the impact of these fluxes on a regional and global scale. For this reason, it is important to understand how global models relate to local measurements.

Here, we present measurements of NO, NO_2, and O_3 taken over two four-week periods in a remote rainforest location from ground and aircraft platforms. We use a global model chemical mechanism implemented in both a global model and a box model to explore the variables that are most important for capturing the diurnal variation of key constituent concentrations at the rainforest site.

In Sect. 2 we present a summary of the measurement techniques and the data. Section 3 examines our ability to reproduce the measurements in two different chemical modelling frameworks. In Sect. 3.1, we use the global model p-TOMCAT at two

different resolutions. In Sect. 3.2, we introduce a box model with the same chemical mechanism as p-TOMCAT and describe sensitivity experiments that investigate uncertainties related to the chemistry and physics. Section 3.3 describes the parameters that give the best fit to the measurements. Finally, Sect. 4 summarizes the study and the results.

2 Measurements

2.1 Methods

Nitrogen oxides and ozone measurements were taken at the Bukit Atur Global Atmospheric Watch (GAW) station (04°58′53″, 117°50′37″, and elevation 426 m). NO measurements were made by chemiluminescence using an Ecophysics CLD 780 TR nitric oxide analyzer, with an Ecophysics PLC 762 NO_2 photolytic converter connected to allow conversion of NO_2 to NO. NO and NO_2 concentrations were measured from an inlet situated at 5 m above ground level through quarter-inch PFA tubing. Measurements were run on continuous sampling except during calibrations and when running zeros. The analyzer was calibrated using an Eco Physics PAG003 pure air generator, an Environs calibration gas blender S6100 and a cylinder of 450 ppbv NO in nitrogen. The photolytic converter efficiency is also determined as part of the calibration. Zero air was run through the system on several occasions to allow more accurate determination of the systematic artefact and detection limit.

Each measurement cycle lasted for 1 min and consisted of 12 s of NO measurement, 12 s of NO_2 measurement and 24 s of interference determination. The remaining 12 s allowed for switching between the different modes and purging of the reaction cell. The 1σ limit of detection for 10 min frequency data was approximately 2.8 pptv for NO and 7 pptv for NO_2.

Ozone concentrations were measured using a Thermo Environmental Instruments (TEI) 49i UV absorption ozone analyzer. The data was internally averaged to one minute frequency and the detection limit was 0.6 ppbv.

On board the FAAM BAe 146 aircraft, NO and NO_2 were measured using the University of East Anglia (UEA) NO_{xy} instrument, which employed the same technique as the ground based instrument described above. Zeros were carried out at the beginning of level runs during the flights and calibrations took place during transit to and from the airport. Detection limits of the UEA NO_{xy} are on the order of 3 pptv for NO and 15 pptv for NO_2 for 10s data, with estimated accuracies of 10% for NO at 1 ppbv and 10% for NO_2 at 1 ppbv. The instrument is described in detail by Brough et al. (2003). Ozone was measured on board the aircraft using a TEI 49C UV absorption analyser.

Isoprene fluxes, used in our box modelling experiments, were measured using a PTR-MS instrument at the Bukit Atur site. Its response was optimized so as to achieve the best compromise between the optimal detection limit for VOCs and the minimization of the impact of high relative humidity. The operational details of the instrument have been presented elsewhere (e.g. Lindinger et al., 1998; de Gouw et al., 2003; Blake et al., 2009) whereas the experimental setup and methodology for OP3 are described in this special issue (Langford et al., 2009).

2.2 Discussion

Time series of NO, NO_2, and O_3 data are shown in Fig. 1. Although the frequency of data collection is 1 min (Sect. 2.1), it is shown here with a running average of 10 min for smoothing purposes. NO levels were typically below 0.1 ppbv, although there were regular spikes above this level which reached up to 0.4 ppbv. NO_2 levels were higher, generally below 0.4 ppbv but reaching 0.8 ppbv. Ozone concentrations ranged from near zero up to 30 ppbv, but were only consistently above 20 ppbv on three days (11–13 April).

Figure 2 shows the median diurnal profiles for the entire April measurement period for all three species[2]. The 25–75 quartile limit is shown in shaded regions around each of the profiles. The ozone diurnal cycle shows a minimum of approximately 6 ppbv around 07:00 h followed by a rise through the morning. Ozone concentrations of approximately 11 ppbv remain until the evening, when concentrations slowly fall to their minimum in the morning. NO_2 concentrations exhibit the most amplified diurnal cycle, which peaks at midnight around 240 pptv and reaches a low of 80 pptv in mid-afternoon. The loss of NO_2 between midnight and midday occurs less rapidly than the buildup between late afternoon and evening. An NO peak of around 70 pptv is observed at 08:00 h and quickly recovers to a fairly constant level between 30 and 40 pptv. This persists until 18:00 h when a further drop to 20 pptv occurs. Non-zero NO concentrations between 15–20 pptv persist throughout the night.

In July, an aircraft joined the campaign in order to make dedicated measurements above the site and over the surrounding areas. On the right side of Fig. 2, the diurnal cycles of NO, NO_2, and O_3 from the ground site at the Bukit Atur GAW tower are shown for this second observation period. These diurnal cycles are sampled only for the four days for which equivalent aircraft data is also available. The average measurements made in profile flight patterns directly over the site are plotted as whiskered points and show values for both boundary layer and free troposphere.

O_3 shows little vertical structure compared to ground measurements. A diurnal structure in the ground based O_3 observations is not clear, with the values around 9 ppbv. Morning aircraft measurements are slightly higher (10–12 ppbv) than the ground based. Aircraft measurements of ozone levels rise slightly to approximately 13 ppbv in the late afternoon, though boundary layer and free troposphere values remain indistinguishable (within uncertainty) from each other.

Boundary layer NO_2 matches the ground based measurements closely, which remain in the range of 100–200 pptv for most of the day. NO_2 measurements show a

[2]A version of this Figure appeared in Hewitt et al. (2009b). The Figure that appears here has higher temporal resolution (10 min data) than the previous version (1 h data).

similar structure (rise until midnight and subsequent decrease afterwards) to the first campaign, but because only four days are sampled here the full diurnal cycle is not shown. NO_2 measurements of around 20 pptv in the free troposphere are much lower than those in the boundary layer and at the surface, demonstrating that NO_2 has a strong vertical structure. NO displays a similar pattern to NO_2 with boundary layer values of 80–200 pptv, that resembles ground-based measurements well, and free tropospheric values that are much lower (less than 10 pptv). The diurnal cycle of NO also bears significant resemblance to that of the first campaign, (i.e. a rise in early morning followed by a slow tapering into the afternoon).

For comparison, the NO concentrations at the ground site in both measurement periods are in between measurements made in the Amazon Rainforest of 20 pptv (Lelieveld et al., 2008) and 100 pptv (Karl et al., 2009). Ozone, on the other hand, is lower at the Borneo site than in reported values for the Amazon for both the boundary layer (19 ppbv) and the free troposphere (37 ppbv) (Lelieveld et al., 2008).

3 Model simulations

In this section, we describe two sets of model simulations. In Sect. 3.1, a global model is used to simulate the diurnal cycle of the three measured species NO, NO_2, and ozone. In Sect. 3.2, we use a box model to explore the chemical and physical parameters influencing the mechanism's performance in replicating observations.

3.1 Global model

3.1.1 Model description

We use the Cambridge global chemistry transport model (CTM) p-TOMCAT to simulate the diurnal cycles of NO, NO_2, and O_3 observed during the April measurement period. The model uses a chemical mechanism implemented in the ASAD chemistry

package (Carver et al., 1997), which is based on the mechanism described in Arnold et al. (2005), has been used in the UM_CAM global model (Zeng et al., 2008; Young et al., 2009), and has recently been incorporated into the United Kingdom Chemistry and Aerosol Model (UKCA, Morgenstern et al., 2008, 2009; O'Connor et al., 2009). It is a medium-size chemistry for a global model, simulating the oxidation of methane, ethane, propane, and isoprene. Isoprene chemistry is simulated using the Mainz isoprene mechanism (MIM) of Pöschl et al. (2000). 81 tracers are carried through 154 bimolecular and 18 termolecular reactions.

The Cambridge p-TOMCAT global CTM is described in more detail in Cook et al. (2007) and Hamilton et al. (2008). The model was used for this study in both a high horizontal resolution mode ($0.56^\circ \times 0.56^\circ$, approximately 62 km in the tropics) and a low resolution mode ($2.8^\circ \times 2.8^\circ$, approximately 310 km in the tropics). Both have 31 levels in the vertical, from the surface to 10 hPa. Both are driven by 6 hourly operational analyses of wind, temperature, and humidity from the European Centre for Medium-range Weather Forecasting (ECMWF). The boundary layer height is diagnosed from input ECMWF operational analyses using the non-local scheme of Holtslag and Boville (1993).

The p-TOMCAT model considers the photolysis of 37 reactions. Photolysis rates are determined by using the Cambridge 2-D model (Law and Pyle, 1993) with the scheme of Hough (1988). This takes account of multiple scattering by clouds using a climatological cloud cover dataset and a fixed aerosol profile. Emissions of NO_x, CO, ethane, propane and isoprene are included. NO_x emissions are added according to the recommendations used in the TAR of the IPCC (Prather et al., 2001) and include industrial, biomass burning, soil, aircraft and lightning emissions. The lightning emissions are scaled to produce 5 Tg N yr^{-1}. A seasonal variation is applied to the biomass burning emissions. Isoprene emissions are taken from the GEIA inventory of Guenther et al. (1995) and have a diurnal cycle applied in the model. Dry deposition velocities are calculated from tabulated velocities based on data from Ganzeveld and Lelieveld (1995) and Zhang et al. (2003) according to the method of Giannakopoulos (1998).

3.1.2 Global model results

Monthly mean diurnal variations for NO, NO_2, and ozone in the boundary layer are shown for both model resolutions in Fig. 3. Both resolutions show a fit for NO which matches the data well; the model reaches a maximum of 65 pptv in the morning around 08:00 h, when the measurement data also peaks (at 60 pptv). At low resolution, there is a dip in midday values to 40 pptv, which was not recorded in the measurements. NO drops to zero around 18:00 h in p-TOMCAT, coinciding with the point when measurement values also drop. As described above, residual NO concentrations of approximately 20 pptv are present throughout the night, and these values are not captured by the global model at either resolution.

The fit to measurements for NO_2 is reasonable for both global models, though the amplitude of the diurnal cycle is slightly too high at 250 pptv, compared with 200 pptv in the measured data. The low resolution version of the model shows constant NO_2 concentrations at night, while the high resolution version of the model shows an increase in NO_2 until dawn. At higher altitude in the model (not shown), NO_2 concentrations are lower (less than 50 pptv) than in the boundary layer levels, which is consistent with the observed vertical profile (Sect. 2.2). We argue below that the measurements, especially during the second half of the night (24:00 to 06:00 h), reflect a large component of free tropospheric character due to mixing during this time. It seems possible that mixing between boundary layer and free tropospheric air in the global model is not sufficient to capture the nighttime decrease in NO_2 shown in the measurements. In addition, the diurnal pattern in both resolutions of the model is slightly too narrow, with a more precipitous decrease in concentrations in the morning and a stronger rise in the evening. In contrast, the measurements show a smoother rise and fall throughout the day and night. Both models capture the rise between 14:00 and 18:00 well.

Finally, the modelled ozone is much too high in both versions of the global model. Concentrations in the low resolution model are around 25 ppbv. The higher resolution model performs slightly better with values of approximately 20 ppbv. In contrast,

measured mixing ratios are between 6 and 11 ppbv. Despite this, the diurnal cycle of the model seems to capture the observed data well. Deposition is an important loss process for ozone and variation in the land surface type, which helps control the deposition rate, can be captured better in the high resolution model. The high resolution version of the model has a much higher resolution land sea mask, and also shows a much stronger land-sea gradient in ozone concentrations than the low resolution version of the model (Fig. 10, Sect. 5, Hewitt et al., 2009b).

3.2 Box model

3.2.1 Model description

We use a stationary box model fitted with the same chemical mechanism as the global model to run a series of sensitivity studies. The chemistry is the same in the two models. Dry deposition in the box model uses the same tabulated values as the global model, but only six species are deposited: NO, NO_2, O_3, peroxy acetyl nitrate (PAN), peroxy-methacrylic nitric anhydride (MPAN), and a lumped nitrate species representing the products from isoprene oxidation (ISON, see Pöschl et al., 2000). The photolysis follows the scheme of the Master Chemical Mechanism (MCM, Saunders et al., 2003). As those photolysis rate constants are originally for July, at 45° N for clear sky conditions, the rate constant for J_{NO_2} was reduced by 50% to account for clouds and aerosol.

Only NO and isoprene are emitted into the box. NO emissions were 600 pptv day^{-1} (the flux is constant) unless otherwise mentioned. Isoprene emissions into the model are taken from ground based flux measurements. Occasionally, flux measurements were not available due to power outages; in these instances, we used linear interpolation to fill in the gaps. In the absence of NO flux measurements at the site, we were not able to constrain NO emissions to a diurnal pattern. NO flux measurements were made in a nearby site underneath the canopy layer Dorsey et al. (2009). In contrast, the Bukit Atur GAW station was in a clearing, and therefore canopy flux measurements are not representative of this site, as there can be a strong difference between below- and

above-canopy fluxes of NO_x (e.g. Duyzer et al., 2004). For these reasons, we assume that NO is emitted constantly into the model; this is also consistent with the emissions used in the global model.

The box model boundary layer height is fixed to a set value during the day (06:00 to 18:00 h) and fixed to a different value at night. For the first set of sensitivity experiments, the daytime boundary layer height was set to 1000 m, and the nighttime height was set to 200 m. The boundary layer height is effectively a mixing depth, and therefore controls the range over which emissions are mixed into the model, and the rate of sinks via deposition.

We set temperature to 25 °C and pressure to a surface value of 1013 mb in the box, appropriate to the conditions of the rainforest site. A 5 °C variation in temperature showed negligible impact on box model output (not shown), so a constant temperature was used. Initial concentrations of chemical species in the box model are set to the values shown in Table 1. NO, NO_2, and O_3 are initialized to their midnight values from the diurnal cycle in the measurements. All other species are initialized to zero.

For the following model-measurement comparisons, both the model and the data are sampled for 15 days to account for day to day variability in isoprene flux measurements.

3.2.2 The base case

Figure 3 shows the initial results from the box model (dark blue line). The box model overestimates NO concentrations (80 pptv instead of 60 pptv), though the structure is decently captured. The shape of the NO_2 curve is very different from the measurements, with NO_2 building up throughout the night. This occurs because any NO emitted into the model reacts with ozone to form NO_2. Ozone is also overestimated in the box model. The box model calculates values of approximately 30 ppbv, with an 8 ppbv diurnal cycle; measurements of 6–11 ppbv are far below this level.

To obtain the "base case" box model run (Fig. 3, light blue line), one key adjustment was made to the original box model output. A dilution parameter was introduced to simulate mixing with the free troposphere resulting from a collapse of the boundary

layer at night. This "venting parameter" removes a small fraction—between 0 and 4 percent—of chemical tracers at each 10 min timestep between 24:00 h and 06:00 h. Doppler lidar measurements of the backscatter from aerosol (Pearson et al., 2009) provide strong evidence for dilution of aerosol in the boundary layer during this period. These measurements were made in a valley next to the Bukit Atur GAW site used for NO_x and ozone measurements in an area of complex topography; the elevation of the lidar measurement site was 198 m (Pearson et al., 2009) compared with 426 m for the Bukit Atur site. The median boundary layer height dropped to approximately 200 m according to these measurements, suggesting that on some nights the Bukit Atur site may have effectively been in the free troposphere. The venting parameter is a simple way to simulate the mixing between the boundary layer box and the free troposphere by parameterizing dilution of species which are concentrated in the boundary layer. As is evident in Fig. 3, the box model was not able to capture the diurnal structure of NO_2 before the introduction of the venting parameter.

The base case (shown in both Figs. 3 and 4) shows both the strengths and weaknesses of the box model with venting. A good fit to the data for NO is obtained, simulating the morning rise in concentration due in part to the onset of photolysis of NO_2. During the day modelled NO follows a similar decay pattern to the measured data, an improvement over the model without venting. Similar to the global model, nighttime NO measurements are not replicated by the box model.

NO_2 measurements and model simulations are in good agreement following the addition of the venting parameter (the base case) and the buildup of NO_2 until midnight and subsequent reduction in concentrations is well captured. At sunrise, when the boundary layer begins to grow, a steep drop in NO_2 concentrations appears around 06:00 h in the box model due to the onset of photolysis. The largest divergence between modelled and measured values occurs in the afternoon, between 12:00 and 16:00 h, though this is still relatively small. Base case modelled and measured ozone display similar diurnal cycles. Both show minima between 07:00 and 08:00 h and maxima in the late afternoon, though the measurements have more structure in the

afternoon than the modelled ozone. However, the box model underestimates the total concentration of ozone, simulating values of 0–8 ppbv instead of 6–11 ppbv.

In summary, the "base case" box model run performs reasonably well, although ozone is too low. The inclusion of the venting parameter, which parameterizes dilution of boundary layer air between 24:00 and 06:00 h, seems necessary in order to simulate the structure of NO_2 measurements at night.

In the next two sections, we describe a series of sensitivity studies in which we explore changes to this base model.

3.2.3 Chemical sensitivities

We have performed a range of sensitivity experiments to explore the model performance. First, a series of emissions sensitivities were carried out (not shown.) In order to determine if the nighttime NO concentration could be captured if emissions were altered, a sensitivity study was performed in which emissions of NO were tripled to 1.8 ppbv day^{-1}. This did not improve the agreement between the modelled and measured values at night. Nonzero nighttime NO could arise from emission taking place very near to the measurement inlet, which is not reproduced by the box model as NO quickly reacts with O_3 to form NO_2 in a zero dimensional model.

We also examined the sensitivity of the model to changing isoprene emissions (not shown). Doubling the emission fluxes into the model reduced NO and NO_2 by approximately 12 pptv during the day, due to sequestration into organic NO_y species. However, the ozone concentration was relatively unaffected. Overall, the diurnal patterns were very similar between the two runs, and between these two studies we determined that the regime was likely not emissions controlled. Although it has been proposed that some chemistry in high-VOC environments might be explained by the presence of unknown reactive hydrocarbons (see Di Carlo et al., 2004, and references therein), any VOC with similar reactivity to that of isoprene seems to be unable to explain any divergence in the model-measurement comparison.

A summary of the various chemical sensitivity runs is shown in Table 2, with corresponding results plotted in Fig. 4. Generally, the diurnal cycle was modelled reasonably well for all the chemical parameters tested and was relatively insensitive to chemical changes. The overall diurnal structure for NO is well captured, with the maxima at 08:00 h. With the inclusion of the venting parameter, the NO_2 diurnal structure is also always well simulated. All the chemical sensitivities capture the cycle of ozone but not the magnitude.

In the first chemical sensitivity test (Fig. 4, aqua line), the photolysis rate of O_3 was reduced by a factor of three. The chemical mechanism shows very little sensitivity to J_{O_3}, barely changing from the base case run. In the second test, ozone deposition velocities (both daytime and nighttime values) were reduced by 75% (Fig. 4, orange line). For ozone, this simulation has the most impact of any of the chemical sensitivity studies, but still does not increase the concentration enough to match measured values. The change in deposition velocities also alters the shape of the diurnal cycle, as nighttime deposition velocities approach a limit of zero.

In an attempt to keep ozone production values high by increasing the concentration of NO_x in the system, an additional simulation was carried out. Recycling of NO_x from the reaction of ISON with OH was modified by increasing the ISON + OH rate constant from 1.3×10^{-11} cm^3 s^{-1} (Chen et al., 1998; Pöschl et al., 2000) to 4.5×10^{-11} cm^3 s^{-1} (Horowitz et al., 2007) (Fig. 4, green line). We also performed an experiment in which NO_x concentrations would decrease; in this sensitivity study, ISON deposition velocity was increased to match nitric acid (Fig. 4, yellow line). Neither experiment has an impact on the modelled values of O_3.

Two computational tests were also performed. In the first, the model species concentrations were reinitialized each day at midnight, rather than using the values calculated by the model the previous day (Fig. 4, red line). This introduced a stronger bias in NO and NO_2 around 06:00 h, the first time photochemistry turns on after reinitialization. A second study reinitializes the model at an artificially high value of ozone, and this too displays a similar model bias at sunrise (Fig. 4, purple line). These two experiments

give confidence that the model sensitivity to initial conditions is eliminated by reusing the concentrations calculated from the previous day.

The six studies discussed emphasize that the results from the UKCA chemical mechanism are relatively robust to chemical, photolytic, and deposition rate changes. As models with this level of complexity, particularly for isoprene oxidation, seem to perform relatively similarly (Archibald et al., 2009; Emmerson and Evans, 2009), it seems plausible that this is not an artefact of the model mechanism itself. From our analysis, it appears likely that the regime is more sensitive to physical processes and parameterizations than chemical ones. In order to assess the impact of these chemistry factors in relation to physical parameters controlling the processes of emission, mixing and deposition, we conducted a further series of experiments based on physical variables.

3.2.4 Physical sensitivities

As shown in Fig. 2, the aircraft data show vertical structure in both NO and NO_2 which display much lower concentrations in the free troposphere compared with the boundary layer. The venting parameter simulates exchange with free tropospheric air at night and assumes that this incoming air has lower concentrations of NO, NO_2, and ozone. However, O_3 displays little to no vertical structure in the measurements. For this reason, a simulation was run in which venting of ozone was turned off while all other species continued to be diluted. Not venting O_3 is the numerical equivalent of removing O_3 and introducing an equal amount during the same amount of time, such that a collapse of the boundary layer and mixing with the free tropospheric air may well bring in "new" ozone, but the concentrations will be similar to the boundary layer air it is replacing. This is reinforced by the difference between the species in their distribution of sources and sinks; NO_x has a source which is largely surface dominated at a remote rainforest location (higher in the troposphere, lightning can contribute as well), whereas ozone has a significant surface sink due to deposition.

Figure 5 shows the results of the box model when ozone is not vented, which displays much better agreement with the measurements. The amplitude of the diurnal cycle of ozone is dampened when O_3 is no longer vented, as the nighttime sinks are reduced. This dampened cycle more closely matches the measured diurnal profile. NO_2 changes little when ozone is not vented, but NO is significantly improved, particularly in the early daytime hours. By keeping O_3 in the box during the night, the chemical sink for NO remains higher, and the elevated values of NO in the morning are correspondingly reduced.

Three variables are used to further test the physical boundaries of the box model: the exact quantity of material lost at night (the venting parameter), the height of the boundary layer during the day, and the height of the boundary layer at night. In order to obtain the best value for these three parameters, a cost function analysis was used:

$$\mathrm{CF}_x = \frac{1}{\mathrm{t}} \sum_{\mathrm{t}} \frac{(|\mathrm{model}_x - \mathrm{measured}_x|)}{\mathrm{measured}_x} \quad (1)$$

where for each species (denoted by x) and at each timestep (t), the difference between modelled and measured values of NO, NO_2, O_3 are evaluated and averaged over a 24 h day and 15 experiment days. The cost function gives the average devation of the model from the measurements expressed as a fraction, where zero is a perfect match. The NO cost function is only evaluated between 06:00 and 18:00 h due to the mechanism's inability to capture nighttime NO concentrations, so that results are not skewed because of nighttime values. The results of the three cost functions are shown in Fig. 6, where a lower value of the cost function represents better agreement between measured and modelled concentrations.

The NO cost function shows a dependence on the venting fraction until the value of 2% per timestep, at which point model and measured data converge to a reasonable agreement of less than 30% difference in value. At the zero value for venting, NO shows almost no dependence on the nighttime boundary layer height, reflecting the fact that we only evaluate the cost function during daytime hours. NO matches the

measurements best (values less than 0.20) for high values of the daytime boundary layer height, though the gradient of dependence on daytime boundary layer height decreases with increasing venting fraction.

At a 0% value for the venting parameter, the NO_2 cost function shows values of 0.30 to 0.80. With venting, the levels are lower (values less than or equal to 0.30), which suggests that the best fit requires at least some material to be removed at night. Between 1% and 4% for the venting parameter, however, NO_2 displays little variation in the cost function, and the entire cost function "space" is valued under 0.30. NO_2 also shows very little dependence on the nighttime boundary layer height, demonstrating that venting is a more important loss process than deposition. The height of the boundary layer during the day is important only at heights less than approximately 700 m.

Ozone was not vented in these experiments, so the cost function for ozone is relatively stable in relation to venting parameter. Ozone shows a very high sensitivity to the boundary layer height during the day (with values ranging between 0.10 and 1.0), presumably due to deposition, and little dependence at night except below 500 m.

3.3 Best fit to measurements

Figure 7 shows the best fit to the measurements obtained using the box model. The values for the venting parameter (2%), boundary layer height during the day (1200 m) and night (750 m) were taken from the cost function analysis minima. The results show good agreement between measured and modelled values, capturing the majority of structure and diurnal variation for all three measured species. NO matches particularly well, though the model is still not able to simulate the residual concentrations at night. These could arise from a highly stratified boundary layer, or rapid mixing times up from the soil to the measurement inlet before chemical reaction[3]. In either case, these

[3]The presence of nighttime NO concentrations will be the subject of a forthcoming paper by Lee et al. (2009). A discussion of nighttime NO can also be found in Pugh et al. (2009)

processes are very small scale, and beyond the capability of a global model (with a resolution of tens to hundreds of kilometres) to capture physically.

Modelled NO_2 is slightly higher than the measured values but captures the structure of the measurements effectively. In particular, the nighttime structure of NO_2 is well simulated once venting was included in the box model. Afternoon NO_2 concentrations are slightly higher in the model than measurements. Since our analysis shows that transport and physical processes dominate the diurnal structure, perhaps this afternoon discrepancy arises from afternoon convection. Ozone looks very similar to measurements, though the rapid rise in the morning is not entirely captured. Nevertheless, the magnitude and basic form of the diurnal cycle are simulated well.

It is possible to crudely adjust the boundary layer scheme in the global model to attempt to reproduce the night time decline in NO_2, a parameterization similar to the box model "venting parameter". The boundary layer in p-TOMCAT varies diurnally in a similar fashion to that seen by the lidar measurements close to Bukit Atur. During daytime the observed boundary layer extends to approximately 1 km but falls to 200 m or less at night (Pearson et al., 2009). In p-TOMCAT, the boundary layer height is similar during the day but at night falls to less than 100 m. The model boundary layer is constrained for numerical stability to be no shallower than the bottom model layer (approximately 30 m). Of course, the global model simulation does not resolve the small scale topography around the measurement site, so we introduced idealized nighttime mixing to simulate the exchange of near surface air with air from above the boundary layer. This new simulation was performed with the diffusion coefficient for the boundary layer increased between midnight and 06:00 h for the bottom three model levels (from the surface to ~300 m) for the gridcell containing the measurement site. Results (not shown) do produce a decrease in NO_2 from midnight, as seen in the box model and the data, as expected, though not for the entire 6 h period. We have not attempted to optimize the mixing; it is nevertheless clear that influx of free tropospheric air could explain the observations in the global model as well as in the box model.

4 Summary

Changes in tropical processes, including land use, biogenic VOC emissions, and soil NO_x emissions are important drivers of global change. To assess these changes, we generally have to run global models at moderate resolutions. In contrast, validation of the global models requires comparison with data representative of much smaller spatial scales.

Data collected during the NERC OP3 field campaign in Sabah, Borneo, present a major opportunity to explore these questions of model validation. How well can a global model chemical mechanism capture the detailed measurements? Here we have used new ground and aircraft data of NO, NO_2, and ozone to address this question. We have compared these measurements with results from a chemical transport model, p-TOMCAT, and the same chemical mechanism included in a box model.

The observed diurnal cycle of NO at the Bukit Atur GAW site showed concentrations between 40 and 60 pptv throughout most of the day, with lower (15–20 pptv) concentrations at night. NO_2 displayed a distinct rise and fall during nighttime, with a peak at midnight. NO_2 concentrations ranged between 100 and 300 pptv. Ozone showed a diurnal pattern with a maximum in the afternoon and a minimum in the early morning. Ozone concentrations were between 6 and 11 ppbv.

The global model displayed decent comparison to the diurnal patterns of NO and NO_2. Residual concentrations of NO at night could not be simulated by any model studied. NO_2 was overestimated during the evening and, especially, before dawn. For ozone, the diurnal cycle was well captured although the concentrations were generally too high. The high resolution model, with a more accurate representation of the land surface and therefore deposition, performed better than the low resolution version of the model, particularly for ozone.

To explore the cause of any differences between p-TOMCAT and the observations, we have used a box model in which a range of chemical and physical sensitivity experiments were performed. These experiments demonstrated that the chemical

mechanism was relatively insensitive to a range of chemical parameters but that modifying the representation of physical processes had a much larger impact. We conclude that the chemical mechanism in our global model, p-TOMCAT, is sufficient to represent the behaviour of the three species considered in detail (NO, NO_2, and ozone), but that discrepancies between model and observations arise from the difficulty of representing physical processes accurately in the global model (especially those related to boundary layer structure). Aerosol backscatter data and the NO_2 nighttime measurements suggest that the surface measurements at the GAW site, when the boundary layer collapses, are influenced significantly by the free troposphere (indeed the site may effectively be in the free troposphere). We cannot expect that the boundary layer scheme, even in the high resolution p-TOMCAT integrations, can capture the details of the boundary layer structure in an area of complex topography, although a preliminary experiment suggests that increased mixing could help replicate the data. The vertical gradient of NO_2, in both the model and the observations, suggests that transport down from the free troposphere is required to explain the observations. In the box model we attempted to represent this by a "venting" parameter and were then able to capture successfully the drop in NO_2 between 24:00 and 08:00 h. In addition, in experiments in which ozone is not vented (because the vertical gradient of ozone is negligible), ozone is reproduced well. Our final "best fit" simulation using the box model closely matches the measurements.

Acknowledgements. The authors would like to acknowledge the OP3 team for their help. We acknowledge the Malaysian and Sabah Governments for permission to conduct research in Malaysia and the Malaysian Meteorological Department (MMD) for access to the Bukit Atur Global Atmosphere Watch tower. We thank the National Environment Research Council for their financial support of the OP3 campaign. B. L. and P. M. thank Brian Davison for his help in transporting and managing equipment. We also acknowledge the National Centre for Atmospheric Science for their support in the development of the model. RCP acknowledges the Gates Cambridge Trust for funding.

References

Archibald, A., Jenkin, M., and Shallcross, D.: An isoprene mechanism intercomparison, Atmos. Environ., doi:10.1016/j.atmosenv.2009.09.016, in press, 2009. 27627

Arnold, S. R., Chipperfield, M. P., and Blitz, M. A.: A three-dimensional model study of the effect of new temperature-dependent quantum yields for acetone photolysis, J. Geophys. Res., 110, D22305, doi:10.1029/2005JD005998, 2005. 27620

Bakwin, P. S., Wofsy, S. C., Fan, S., Keller, M., Trumbore, S. E., and Costa, J. M. D.: Emission of nitric oxide (NO) from tropical forest soils and exchange of NO between the forest canopy and atmospheric boundary layers, J. Geophys. Res., 95, 16755–16764, 1990. 27615

Blake, R. S., Monks, P. S., and Ellis, A. M.: Proton-Transfer Reaction Mass Spectrometry, Chem. Rev., 109, 861–896, 2009. 27617

Brough, N., Reeves, C. E., Penkett, S. A., Stewart, D. J., Dewey, K., Kent, J., Barjat, H., Monks, P. S., Ziereis, H., Stock, P., Huntrieser, H., and Schlager, H.: Intercomparison of aircraft instruments on board the C-130 and Falcon 20 over southern Germany during EXPORT 2000, Atmos. Chem. Phys., 3, 2127–2138, 2003, http://www.atmos-chem-phys.net/3/2127/2003/. 27617

Carver, G. D., Brown, P. D., and Wild, O.: The ASAD atmospheric chemistry integration package and chemical reaction database, Comput. Phys. Commun., 105, 197–215, doi:10.1016/S0010-4655(97)00056-8, 1997. 27620

Chen, X., Hulbert, D., and Shepson, P. B.: Measurement of the organic nitrate yield from OH reaction with isoprene, J. Geophys. Res., 103, 25563–25568, 1998. 27626

Cook, P. A., Savage, N. H., Turquety, S., Carver, G. D., O'Connor, F. M., Heckel, A., Stewart, D., Whalley, L. K., Parker, A. E., Schlager, H., Singh, H. B., Avery, M. A., Sachse, G. W., Brune, W., Richter, A., Burrows, J. P., Purvis, A. C., Lewis, A. C., Reeves, C. E., Monks, P. S., Levine, J. G., and Pyle, J. A.: Forest fire plumes over the North Atlantic: p-TOMCAT model simulations with aircraft and satellite measurements from the ITOP/ICARTT campaign, J. Geophys. Res., 112, D10S43, doi:0.1029/2006JD007563, 2007. 27620

Crutzen, P. J.: A discussion of the chemistry of some minor constituents in the stratosphere and troposphere, Pure Appl. Geophys., 106, 1385–1399, doi:10.1007/BF00881092, 1973. 27614

de Gouw, J., Warneke, C., Karl, T., Eerdekens, G., van der Veen, C., and Fall, R.: Sensitivity and specificity of atmospheric trace gas detection by proton-transfer-reaction mass spectrometry,

Int. J. Mass Spectrom., 223–224, 365–382, 2003. 27617

Delon, C., Reeves, C. E., Stewart, D. J., Serça, D., Dupont, R., Mari, C., Chaboureau, J.-P., and Tulet, P.: Biogenic nitrogen oxide emissions from soils impact on NO_x and ozone over West Africa during AMMA (African Monsoon Multidisciplinary Experiment): modelling study, Atmos. Chem. Phys., 8, 2351–2363, 2008, http://www.atmos-chem-phys.net/8/2351/2008/. 27615

Di Carlo, P., Brune, W. H., Martinez, M., Harder, H., Lesher, R., Ren, X., Thornberry, T., Carroll, M. A., Young, V., Shepson, P. B., Riemer, D., Apel, E., and Campbell, C.: Missing OH reactivity in a forest: Evidence for unknown reactive biogenic VOCs, Science, 304, 722–724, doi:10.1126/science.1094392, 2004. 27625

Dorsey, J. R. and Gallagher, M. W.: Observations of soil NO_x emission from a Southeast Asian rainforest: a technique to assess biological controls, Atmos. Chem. Phys. Discuss., in preparation, 2010. 27622

Duyzer, J. H., Dorsey, J. R., Gallagher, M. W., Pilegaard, K., and Walton, S.: Oxidized nitrogen and ozone interaction with forests. II: Multi-layer process-oriented modelling results and a sensitivity study for Douglas fir, Q. J. Roy. Meteorol. Soc., 130, 1957–1971, 2004. 27623

Emmerson, K. M. and Evans, M. J.: Comparison of tropospheric chemistry schemes for use within global models, Atmos. Chem. Phys., 9, 1831–1845, 2009, http://www.atmos-chem-phys.net/9/1831/2009/. 27627

Forster, P. M. D., Johnson, C. E., Law, K. S., Pyle, J. A., and Shine, K. P.: Further estimates of radiative forcing due to tropospheric ozone changes, Geophys. Res. Lett., 23, 3221–3324, 1996. 27614

Franzblau, E. and Popp, C. J.: Nitrogen oxides produced from lightning, J. Geophys. Res., 94, 11089–11104, 1989. 27615

Fuglestvedt, J. S., Berntsen, T. K., Isaksen, I. S. A., Mao, H., Liang, X.-L., and Wang, W.-C.: Climatic forcing of nitrogen oxides through changes in tropospheric ozone and methane; global 3D model studies, Atmos. Environ., 33, 961–977, doi:10.1016/S1352-2310(98)00217-9, 1999. 27614

Ganzeveld, L. and Lelieveld, J.: Dry deposition parametisation in a chemistry general circulation model and its influence on the distribution of reactive trace gases, J. Geophys. Res., 100, 20999–21012, doi:10.1029/95JD02266, 1995. 27620

Gauss, M., Myhre, G., Isaksen, I. S. A., Grewe, V., Pitari, G., Wild, O., Collins, W. J., Dentener, F. J., Ellingsen, K., Gohar, L. K., Hauglustaine, D. A., Iachetti, D., Lamarque, J.-F., Mancini,

E., Mickley, L. J., Prather, M. J., Pyle, J. A., Sanderson, M. G., Shine, K. P., Stevenson, D. S., Sudo, K., Szopa, S., and Zeng, G.: Radiative forcing since preindustrial times due to ozone change in the troposphere and the lower stratosphere, Atmos. Chem. Phys., 6, 575–599, 2006,
http://www.atmos-chem-phys.net/6/575/2006/. 27614

Giannakopoulos, C.: Modelling the impact of physical and removal processes on tropospheric chemistry, Ph.D. thesis, University of Cambridge, 1998. 27620

Guenther, A., Hewitt, C. N., Erickson, D., Fall, R., Geron, C., Graedel, T., Harley, P., Klinger, L., Lerdau, M., McKay, W. A., Pierce, T., Scoles, B., Steinbrecher, R., Tallaamraju, R., Taylor, J., and Zimmerman, P.: A global model of natural volatile organic compound emissions, J. Geophys. Res., 100, 8873–8892, 1995. 27620

Hamilton, J. F., Allen, G., Watson, N. M., Lee, J. D., Saxton, J. E., Lewis, A. C., Vaughan, G., Bower, K. N., Flynn, M. J., Crosier, J., Carver, G. D., Harris, N. R. P., Parker, R. J., Remedios, J. J., and Richards, N. A. D.: Observations of an atmospheric chemical equator and its implications for the tropical warm pool region, J. Geophys. Res., 113, D20313, doi:10.1029/2008JD009940, 2008. 27620

Hewitt, C. N., MacKenzie, A. R., Di Carlo, P., Di Marco, C. F., Dorsey, J. R., Evans, M., Fowler, D., Gallagher, M. W., Hopkins, J. R., Jones, C. E., Langford, B., Lee, J. D., Lewis, A. C., Lim, S. F., McQuaid, J., Misztal, P., Moller, S. J., Monks, P. S., Nemitz, E., Oram, D. E., Owen, S. M., Phillips, G. J., Pugh, T. A. M., Pyle, J. A., Reeves, C. E., Ryder, J., Siong, J., Skiba, U., and Stewart, D. J.: Nitrogen management is essential to prevent tropical oil palm plantations from causing ground-level ozone pollution, Proc. Natl. Acad. Sci. USA, 106, 18447–18451, doi:10.1073/pnas.0907541106, 2009a. 27614

Hewitt, C. N., Lee, J., Barkley, M. P., Carslaw, N., Chappell, N. A., Coe, H., Collier, C., Commane, R., Davies, F., DiCarlo, P., Di Marco, C. F., Edwards, P. M., Evans, M. J., Fowler, D., Furneaux, K. L., Gallagher, M., Guenther, A., Heard, D. E., Helfter, C., Hopkins, J., Ingham, T., Irwin, M., Jones, C., Karunaharan, A., Langford, B., Lewis, A. C., Lim, S. F., MacDonald, S. M., MacKenzie, A. R., Mahajan, A. S., Malpass, S., McFiggans, G., Mills, G., Misztal, P., Moller, S., Monks, P. S., Nemitz, E., Nicolas-Perea, V., Oetjen, H., Oram, D., Palmer, P. I., Phillips, G. J., Plane, J. M. C., Pugh, T., Pyle, J. A., Reeves, C. E., Robinson, N. H., Stewart, D., Stone, D., and Whalley, L. K.: Oxidant and particle photochemical processes above a south-east Asian tropical rain forest (the OP3 project): introduction, rationale, location characteristics and tools, Atmos. Chem. Phys., submitted, 2009b. 27613, 27614, 27618, 27622

Holton, J. R., Haynes, P. H., McIntyre, M. E., Douglass, A. R., Rood, R. B., and Pfister, L.: Stratosphere-troposphere exchange, Rev. Geophys., 33, 403–439, 1995. 27615

Holtslag, A. and Boville, B.: Local Versus Nonlocal Boundary-Layer Diffusion in a Global Climate Model, J. Climate, 6, 1825–1842, 1993. 27620

Horowitz, L. W., Fiore, A. M., Milly, G. P., Cohen, R. C., Perring, A., Wooldridge, P. J., Hess, P. G., Emmons, L. K., and Lamarque, J.-F.: Observational constraints on the chemistry of isoprene nitrates over the eastern United States, J. Geophys. Res., 112, D12S08, doi:10.1029/2006JD007747, 2007. 27626, 27641

Hough, A.: The calculation of photolysis rates for use in global tropospheric modelling studies, AERE Report 13259, At. Energy Res. Estab., Harwell, UK, 1988. 27620

Jaeglé, L., Martin, R. V., Chance, K., Steinberger, L., Kurosu, T. P., Jacob, D. J., Modi, A. I., Yobou, V., Sigha-Nkamdjou, L., and Galy-Lacaux, C.: Satellite mapping of rain-induced nitric oxide emissions from soils, J. Geophys. Res., 109, D21310, doi:10.1029/2004JD004787, 2004. 27615

Jenkin, M. E. and Clemitshaw, K. C.: Ozone and other secondary photochemical pollutants: Chemical processes governing their formation in the planetary boundary layer, Atmos. Environ., 34, 2499–2527, doi:10.1016/S1352-2310(99)00478-1, 2000. 27614

Jerrett, M., Burnett, R. T., Pope, C. Arden, I., Ito, K., Thurston, G., Krewski, D., Shi, Y., Calle, E., and Thun, M.: Long-Term Ozone Exposure and Mortality, N. Engl. J. Med., 360, 1085–1095, 2009. 27614

Karl, T., Guenther, A., Turnipseed, A., Tyndall, G., Artaxo, P., and Martin, S.: Rapid formation of isoprene photo-oxidation products observed in Amazonia, Atmos. Chem. Phys., 9, 7753–7767, 2009,
http://www.atmos-chem-phys.net/9/7753/2009/. 27619

Kasibhatla, P. S.: NO_y from Sub-Sonic Aircraft Emissions: A Global Three-Dimensional Model Study, Geophys. Res. Lett., 20, 1707–1710, 1993. 27615

Kuhn, U., Andreae, M. O., Ammann, C., Araújo, A. C., Brancaleoni, E., Ciccioli, P., Dindorf, T., Frattoni, M., Gatti, L. V., Ganzeveld, L., Kruijt, B., Lelieveld, J., Lloyd, J., Meixner, F. X., Nobre, A. D., Pöschl, U., Spirig, C., Stefani, P., Thielmann, A., Valentini, R., and Kesselmeier, J.: Isoprene and monoterpene fluxes from Central Amazonian rainforest inferred from tower-based and airborne measurements, and implications on the atmospheric chemistry and the local carbon budget, Atmos. Chem. Phys., 7, 2855–2879, 2007,

http://www.atmos-chem-phys.net/7/2855/2007/. 27614
Langford, B., Misztal, P., Nemitz, E., Davison, B., Helfter, C., Lee, J., MacKenzie, A. R., and Hewitt, C. N. Fluxes of volatile organic compounds from a south-east Asian tropical rainforest, Atmos. Chem. Phys. Discuss., in preparation, 2010. 27617
Law, K. S. and Pyle, J. A.: Modeling trace gas budgets in the troposphere 1. Ozone and odd nitrogen, J. Geophys. Res., 98, 18377–18400, 1993. 27620
Lee, J. et al.: NO_x above a tropical rainforest, in preparation, Atmos. Chem. Phys., 2009. 27629
Lelieveld, J., Butler, T. M., Crowley, J. N., Dillon, T. J., Fischer, H., Ganzeveld, L., Harder, H., Lawrence, M. G., Martinez, M., Taraborrelli, D., and Williams, J.: Atmospheric oxidation capacity sustained by a tropical forest, Nature, 452, 737–740, doi:10.1038/nature06870, 2008. 27614, 27619
Levy II, H., Moxim, W. J., Klonecki, A. A., and Kasibhatla, P. S.: Simulated tropospheric NO_x : Its evaluation, global distribution and individual source contributions, J. Geophys. Res., 104, 26279–26306, 1999. 27615
Lindinger, W., Hansel, A., and Jordan, A.: On-line monitoring of volatile organic compounds at pptv levels by means of proton-transfer-reaction mass spectrometry (PTR-MS) medical applications, food control and environmental research, Int. J. Mass Spectrom. Ion Proc., 173, 191–241, 1998. 27617
Liu, S. C., Trainer, M., Fehsenfeld, F. C., Parrish, D. D., Williams, E. J., Fahey, D. W., Hübler, G., and Murphy, P. C.: Ozone production in the rural troposphere and the implications for regional and global ozone distributions, J. Geophys. Res., 92, 4191–4207, 1987. 27614
Morgenstern, O., Braesicke, P., Hurwitz, M. M., O'Connor, F. M., Bushell, A. C., Johnson, C. E., and Pyle, J. A.: The World Avoided by the Montreal Protocol, Geophys. Res. Lett., 35, L16811, doi:10.1029/2008GL034590, 2008. 27620
Morgenstern, O., Braesicke, P., O'Connor, F. M., Bushell, A. C., Johnson, C. E., Osprey, S. M., and Pyle, J. A.: Evaluation of the new UKCA climate-composition model Part I: The stratosphere, Geoscientific Model Development, 2, 43–57, 2009. 27620
O'Connor, F. M., Johnson, C. E., Morgenstern, O., and Collins, W. J.: Interactions between tropospheric chemistry and climate model temperature and humidity biases, Geophys. Res. Lett., 36, L16 801, 2009. 27620
Pearson, G., Davies, F., and Collier, C.: Remote sensing of the tropical rain forest boundary layer using pulsed Doppler lidar, in preparation, Atmos. Chem. Phys., 2009. 27624, 27630
Pöschl, U., von Kulhmann, R., Poisson, N., and Crutzen, P. J.: Development and

intercomparison of condensed isoprene oxidation mechanisms for global atmospheric modelling, J. Atmos. Chem., 37, 29–52, doi:10.1023/A:1006391009798, 2000. 27620, 27622, 27626
Prather, M., Ehhalt, D., Dentener, F., Derwent, R., Dlugokencky, E., Holland, E., Isaksen, I., Katima, J., Kirchoff, V., Matson, P., Midgley, P., and Wang, M.: Climate Change 2001: The Scientific Basis, chap. Atmospheric chemistry and greenhouse gases, Cambridge University Press, Cambridge, UK, 239–287, 2001. 27620
Pugh, T. A. M., MacKenzie, A. R., Hewitt, C. N., Langford, B., Edwards, P. M., Furneaux, K. L., Heard, D. E., Hopkins, J. R., Jones, C. E., Karunaharan, A., Lee, J., Mills, G., Misztal, P., Moller, S., Monks, P. S., and Whalley, L. K.: Simulating atmospheric composition over a South-East Asian tropical rainforest: Performance of a chemistry box model, Atmos. Chem. Phys., in preparation, 2009. 27629
Saunders, S. M., Jenkin, M. E., Derwent, R. G., and Pilling, M. J.: Protocol for the development of the Master Chemical Mechanism, MCM v3 (Part A): Tropospheric degradation of non-aromatic volatile organic compounds, Atmos. Chem. Phys., 3, 161–180, 2003, http://www.atmos-chem-phys.net/3/161/2003/. 27622
Schumann, U. and Huntrieser, H.: The global lightning-induced nitrogen oxides source, Atmos. Chem. Phys., 7, 3823–3907, 2007, http://www.atmos-chem-phys.net/7/3823/2007/. 27615
Sillman, S.: The use of NO_y, H_2O_2, and HNO_3 as indicators for ozone-NO_x-hydrocarbon sensitivity in urban locations, J. Geophys. Res., 100, 14175–14188, 1995. 27614
Sillman, S., Logan, J. A., and Wofsy, S. C.: The sensitivity of ozone to nitrogen oxides and hydrocarbons in regional ozone episodes, J. Geophys. Res., 95, 1837–1851, 1990. 27614
Steinkamp, J., Ganzeveld, L. N., Wilcke, W., and Lawrence, M. G.: Influence of modelled soil biogenic NO emissions on related trace gases and the atmospheric oxidizing efficiency, Atmos. Chem. Phys., 9, 2663–2677, 2009, http://www.atmos-chem-phys.net/9/2663/2009/. 27615
Stevenson, D. S., Dentener, F. J., Schultz, M. G., Ellingsen, K., van Noije, T. P. C., Wild, O., Zeng, G., Amann, M., Atherton, M., Bell, N., Bergmann, D. J., Bey, I., Bulter, T., Cofala, J., Collins, W. J., Derwent, R. G., Doherty, R. M., Drevet, J., Eskes, H. J., Fiore, A. M., Gauss, M., Hauglustaine, D. A., Horowitz, L. W., Isaksen, I. S. A., Krol, M. C., Lamarque, J.-F., Lawrence, M. G., Montanaro, V., Müller, J. F., Pitari, G., Prather, M. J., Pyle, J. A., Rast, S., Rodriguez, J. M., Sanderson, M. G., Savage, N. H., Shindell, D. T., Strahan, S. E., Sudo, K., and Szopa,

S.: Multimodel ensemble simulations of present-day and near-future tropospheric ozone, J. Geophys. Res., 111, D08301, doi:10.1029/2005JD006338, 2006. 27614, 27615

Toenges-Schuller, N., Stein, O., Rohrer, F., Wahner, A., Richter, A., Burrows, J. P., Beirle, S., Wagner, T., Platt, U., and Elvidge, C. D.: Global distribution pattern of anthropogenic nitrogen oxide emissions: Correlation analysis of satellite measurements and model calculations, J. Geophys. Res., 111, D05312, doi:10.1029/2005JD006068, 2006. 27615

van Dingenen, R., Dentener, F. J., Raes, F., Krol, M. C., Emberson, L., and Cofala, J.: The global impact of ozone on agricultural crop yields under current and future air quality legislation, Atmos. Environ., 43, 604–618, 2009. 27614

Wild, O.: Modelling the global tropospheric ozone budget: exploring the variability in current models, Atmos. Chem. Phys., 7, 2643–2660, 2007, http://www.atmos-chem-phys.net/7/2643/2007/. 27615

Wilkins, C. K., Clausen, P. A., Wolkoff, P., Larsen, S., Hammer, M., Larsen, K., Hansen, V., and Nielsen, G. D.: Formation of strong airway irritants in mixtures of isoprene/ozone and isoprene/ozone/nitrogen dioxide, Environ. Health Persp., 109, 937–941, 2001. 27614

Yienger, J. J. and Levy II, H.: Empirical model of global soil-biogenic NO_x emissions, J. Geophys. Res., 100, 11477–11464, 1995. 27615

Young, P., Arneth, A., Schurgers, G., Zeng, G., and Pyle, J. A.: The CO_2 inhibition of terrestrial isoprene emission significantly affects future ozone projections, Atmos. Chem. Phys., 9, 2793–2803, 2009, http://www.atmos-chem-phys.net/9/2793/2009/. 27620

Zeng, G., Pyle, J. A., and Young, P. J.: Impact of climate change on tropospheric ozone and its global budgets, Atmos. Chem. Phys., 8, 369–387, 2008, http://www.atmos-chem-phys.net/8/369/2008/. 27620

Zhang, L., Brook, J. R., and Vet, R.: A revised parametisation for gaseous dry deposition in air-quality models, Atmos. Chem. Phys., 3, 2067–2082, 2003, http://www.atmos-chem-phys.net/3/2067/2003/. 27620

Table 1. Initial concentrations of six species used in the box model.

Species	Concentration
CO	130 ppbv
HOOH	3 ppbv
C_2H_6	500 pptv
C_3H_8	50 pptv
HCHO	1 ppbv
CH_3COCH_3	50 pptv

Table 2. Summary of chemical sensitivity tests

Short name	Fig. Colour	Description
Base	Light Blue	The base case
O3 phot	Aqua	J_{O_3} divided by 3
Vd O3	Orange	Ozone deposition velocities reduced by 75%
Horowitz	Green	NO_x recycling rates as Horowitz et al. (2007)
ISON dep	Yellow	ISON tracer deposition velocities set equal to those of PAN
Reinit	Red	Reinitialized the model each day at midnight
Init O3=9	Purple	Reinitialized at midnight with 9 ppbv O_3

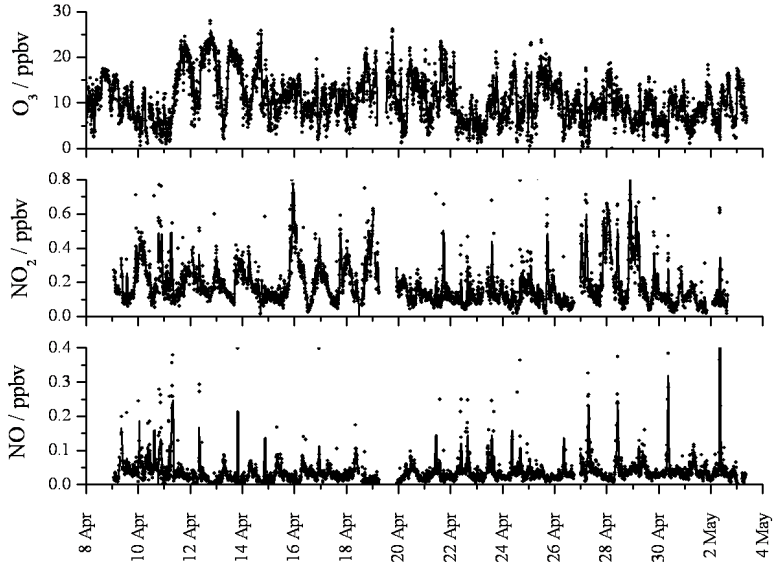

Fig. 1. Time series of measured NO, NO_2, and O_3 at the Bukit Atur GAW ground site, plotted versus local time (GMT + 8).

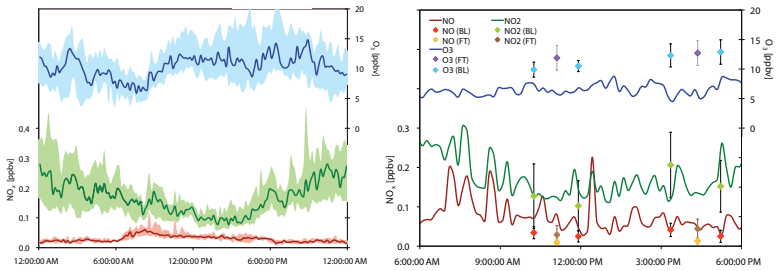

Fig. 2. Left: Median diurnal cycle of ground-based measured NO (dark red), NO_2 (dark green), and O_3 (dark blue) in April. The corresponding 25–75 quartile interval is shown with each measurement: NO in pink, NO_2 in light green, and O_3 in light blue. Right: median diurnal measurements in July, shown only for the days when corresponding flight data is available between 06:00 and 18:00 h; diurnal profiles are the same color. Average flight data for morning and afternoon profiles above the site are shown as whiskered points and are separated by height. NO boundary layer measurements are show in red (boundary layer) and yellow (free troposphere). NO_2 is shown in light green (boundary layer) and brown (free troposphere). O_3 is shown in light blue (boundary layer) and purple (free troposphere).

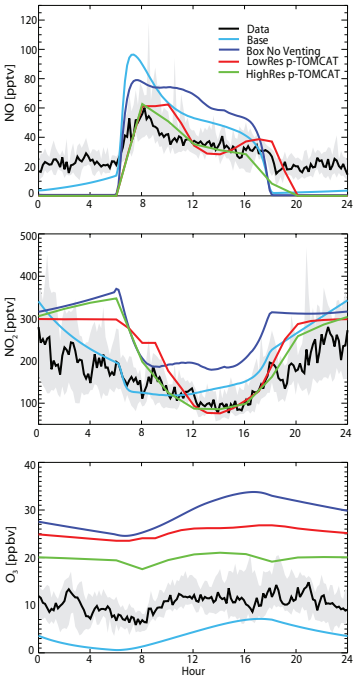

Fig. 3. Global and box model comparison to diurnal cycle of NO, NO_2, and O_3 from the median diurnal cycle in the measurements (black, with 25–75 quartile in grey). The global model is shown in red (low resolution) and green (high resolution) for the lowest model level, and the box model is shown dark blue (without venting) and light blue (the "base case").

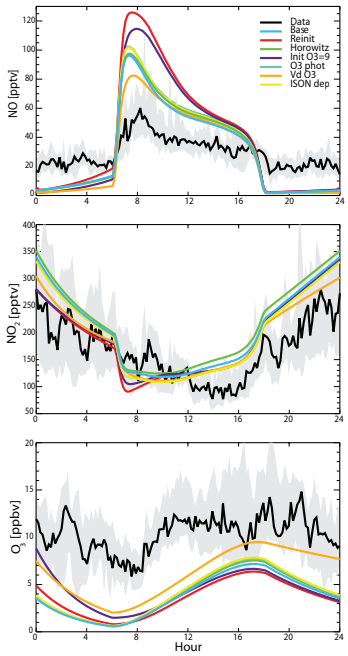

Fig. 4. 15 day average diurnal **(a)** NO [pptv], **(b)** NO_2 [pptv], **(c)** and O_3 [ppbv] from measurements (black) with 75% confidence intervals shown in the shaded grey. Seven model experiments are overlaid in various colours: the base run is shown in light blue, reduction of ozone photolysis rate is shown in dark blue, reduction of ozone deposition velocities is shown in orange, adjustment of NO_xrecycling rates is shown in green, ISON deposition change is shown in yellow, reinitialisation at midnight is shown in red, and reinitialisation with high ozone is shown in purple.

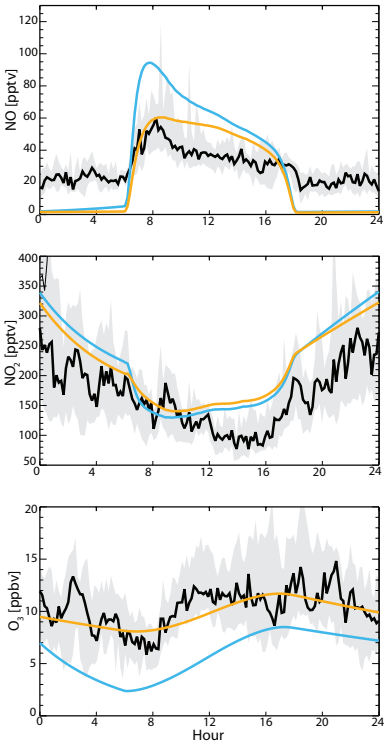

Fig. 5. Model comparison to diurnal cycle of NO **(a)**, NO_2 **(b)**, and O_3 **(c)** without (orange) and with (the base case, blue) venting ozone.

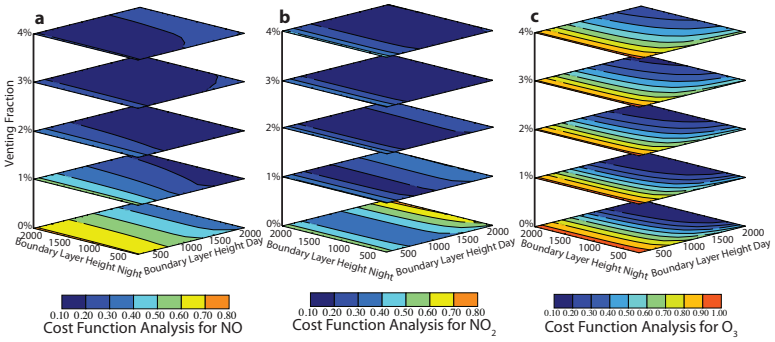

Fig. 6. Cost function [|%| difference] of model-measurement comparison to diurnal average **(a)** NO, **(b)** NO_2, and **(c)** O_3. See text for a description of the cost function.

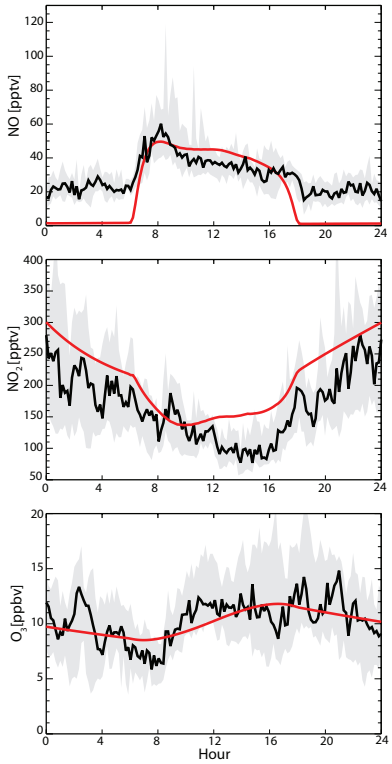

Fig. 7. Red: Best fit box model comparison to diurnal average medians of **(a)** NO, **(b)** NO_2, and **(c)** O_3after adjustments to the venting parameter and boundary layer heights.